Rheological behavior of Pluronic/Pluronic diacrylate hydrogels used for bacteria encapsulation in living materials

Shardul Bhusari[1,2], Maxi Hoffmann[3], Petra Herbeck-Engel[1], Shrikrishnan Sankaran[1], Manfred Wilhelm[3], Aránzazu del Campo [1,2]*

[1] INM-Leibniz Institute for New Materials, Campus D2 2, 66123 Saarbrücken, Germany

[2] Chemistry Department, Saarland University, 66123 Saarbrücken, Germany

[3] Karlsruhe Institute of Technology (KIT), Institute for Chemical Technology and Polymer Chemistry (ITCP), Engesserstraße 18, 76131 Karlsruhe, Germany

**Corresponding author: aranzazu.delcampo@leibniz-inm.de*

Keywords: Pluronic hydrogel, bacteria encapsulation, engineered living materials, bacteria mechanobiology, bacteria-material interactions

Abstract

Pluronic (Plu)-based hydrogels containing a fraction of Pluronic diacrylate (PluDA) chains form physical networks with additional covalent crosslinks. These hydrogels have been used to encapsulate bacteria or yeast in living materials and devices. Within Plu/PluDA hydrogels, the growth of the encapsulated organisms decreases with increasing density of covalent bonds. This has been attributed to the capability of the organisms to sense and respond to the mechanical properties of the embedding matrix. Here we investigate the rheological behavior of 30 wt% Plu/PluDA hydrogels with increasing covalent crosslinking adjusted by the PluDA fraction in the mixture. This hydrogel composition allowed hydrogel-regulated growth of *E. coli* in living devices in previous reports. We aim to find experimental descriptors of the hydrogel's rheological response that can be correlated to the reported growth behavior. We present stress relaxation and creep-recovery experiments and quantify the elastic, viscoelastic and plastic responses of the hydrogels as function of the covalent crosslinking degree, with a focus on critical yield strain/stress and relaxation parameters. An

inverse correlation was observed between the storage modulus and the critical stress/strain for fluidization τ_F, of the hydrogel and the reported maximum volume of *E. coli* colonies grown in the hydrogels. These results contribute to the biophysical understanding of bacteria behavior in confinement and are relevant for different application contexts, eg. to improve the performance and safety of living therapeutic implants and to maximize the yield of biotechnological production in immobilized cell reactors.

Statement of significance

Pluronic-based hydrogels are increasingly used to encapsulate bacteria and yeast in engineered living materials (ELMs). The mechanical properties of these hydrogels impact the growth of the organisms in the confined state. This study presents a fundamental characterization of the viscoelastic response of Pluronic and Pluronic diacrylate hydrogels with different degrees of covalent crosslinking by rheology. It correlates rheological response with observed cell behavior in model encapsulated systems, thereby contributing to the understanding of bacteria-material interactions and their impact in ELMs.

1 Introduction

Soft hydrogel networks with combined physical (dynamic) and covalent (permanent) crosslinks are interesting materials for the encapsulation and controlled expansion of cells.[2] The inherent reorganization capability of the dynamic crosslinks allows cells to deform the surrounding material as they proliferate and accommodate daughter cells. In parallel, the elastic network imposes increasing compressive forces on the cell population as it grows.[3] The magnitude of the compressive force regulates the size and morphology of the cellular aggregates and depends on the viscoelastic properties of the hydrogel network (**Scheme 1a**).[4] Pluronic (PEO_x-PPO_y-PEO_x) hydrogels have been adopted as model biocompatible hydrogel to embed bacteria and yeast.[5][6][7][8] Pluronic (Plu) hydrogels are

physical networks stabilized by reversible interactions. By mixing with Pluronic diacrylate (PluDA), covalent crosslinks are introduced in the network structure without disturbing the physical crosslinks. We recently reported that the growth rate of bacteria colonies embedded in Plu/PluDA hydrogels decreases as the degree of covalent crosslinks in the network increases.[1] This behavior was attributed to the associated changes in the mechanical properties of the embedding hydrogel network.[1] Although the trend has been seen by other authors and in other systems,[9] the details on the interplay between hydrogel mechanical response and growth of embedded bacteria remain to be clarified.[10]

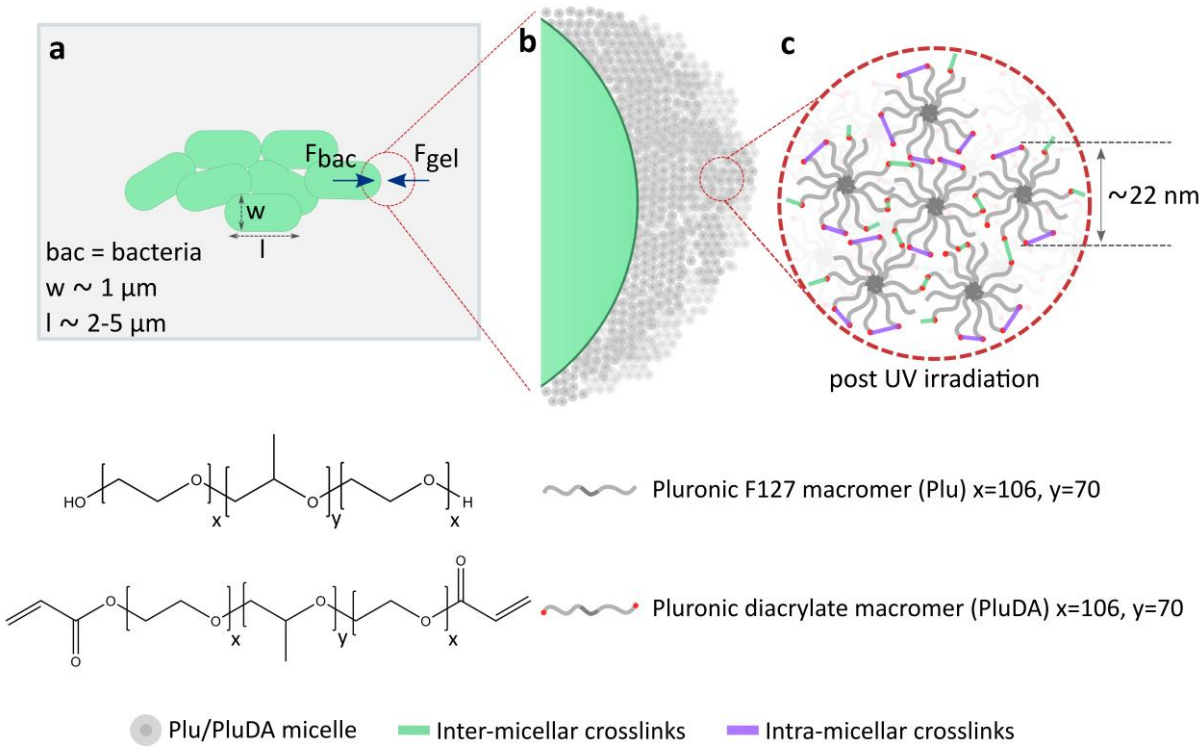

Scheme 1: **a)** Representation of a growing bacteria colony embedded in Pluronic/Pluronic diacrylate hydrogel; **b)** Micellar structure of the Plu/PluDA hydrogel above the sol-gel transition temperature. The micelles have a diameter of ca. 22 nm and build aggregates that form a network. **c)** Micellar structure representing the organization of the PEOx-PPOy-PEOx triblock copolymer chains in the micelles and the inter- and intra-micellar covalent crosslinks between PluDA chains.

Physical Pluronic hydrogels are formed by aggregation of the Pluronic micelles into clusters through the interactions between the PEO coronas (**Scheme 1b,c**). Above the transition temperature, the micellar clusters grow and build a 3D network.[11][12] For the specific Pluronic F127 (PEO_{106}-PPO_{70}-PEO_{106}), which will be used in the experiments in this article, the critical micellar concentration (cmc) is at 0.725 wt. % in water at 25 °C[13][14][15], and the sol-gel transition occurs at polymer concentrations > 5 wt. % and temperatures above 14 °C. The assembly of Pluronic F127 chains in 3D networks has been studied by scattering methods like dynamic light scattering (DLS) and small angle neutron scattering (SANS).[16][17] The order of the micelles in the clusters depends on external conditions (i.e., temperature, salt concentration, shear forces)[18][17] and ranges from perfect face-centered cubic (FCC) or hexagonally close packed (HCP) structures to random stackings. As associative physical networks, Pluronic hydrogels show elastic properties in the quiescent state and undergo yielding, i.e. fracture and flow, when the stress surpasses the interparticle forces.[19][20] The shear thinning behavior and the thermosensitivity makes Pluronic gels interesting from a biomedical perspective.[21] It allows them to be easily processed, mixed with payloads, and injected for application in drug delivery and for replacing biological fluids.[22][23][24]

Physical Pluronic hydrogels swell and dissociate into individual micelles when immersed in water. The introduction of polymerizable acrylate functionalities as end-groups of the Pluronic chains provides the possibility to stabilize the micellar hydrogel via the formation of permanent, covalent bonds between the micelles.[6][12] Covalent crosslinking affects the mechanical behavior, specially the elasticity as quantified via G' of the hydrogel.[1] By varying the PluDA fraction in Plu/PluDA hydrogels the density of chemical crosslinks in the hydrogel and the resulting mechanical properties can be tuned. For example, a 30 wt. %

Plu/PluDA hydrogels show increasing elastic response (G') (from 17.8 ± 1.4 to 42.9 ± 1.9 kPa) and decreasing non-elastic response (from creep-recovery curves) when the PluDA fraction in the mixture increased from 0 to 100%.[1]

Here, we present a detailed study of the time-dependent rheological behavior of Plu/PluDA hydrogels as a function of PluDA fraction. We use 30 wt. % Plu/PluDA hydrogels as used in preceeding reports in the fabrication of living therapeutic devices by different groups. [5][6][25] We aim to provide information on the mechanical response of Plu/PluDA hydrogels to progress in our understanding of how it correlates with the behavior of encapsulated organisms.[5][7][8][25][26]

2 Materials and Methods

2.1 Sample preparation

Pluronic diacrylate (PluDA) was synthesized by reaction of Pluronic F127 (Plu) with acryloyl chloride in the presence of triethylamine according to a reported protocol.[31] Acrylation degrees of 70% were typically obtained. The conditions for DAX gel preparation were taken from a previous report.[1] In short, 30 wt. % Plu and PluDA stock solutions (named DA0 and DA100, respectively) were prepared in milliQ water and contained 0.2% w/v Irgacure 2959 (Sigma-Aldrich Co.) as photoinitiator. Solutions were stored at 4 °C. DA 25, DA 50 and DA 75 hydrogels were prepared by mixing DA0 and DA100 stock solutions in the following ratios- 3:1 (DA 25), 1:1 (DA 50) and 1:3 (DA 75). After mixing, the DAX hydrogels were allowed to form at room temperature for 10 minutes.[47] For the photoinitiated crosslinking, hydrogels were exposed to UV light (365 nm, 6 mW/cm^2) using a OmniCure Series 1500 lamp for 60 s through a UV transparent bottom plate for rheology.

2.2 Raman spectroscopy of Plu/PluDA powders and DA 0-100 hydrogels

Raman investigations were carried out at ambient conditions on a LabRAM HR Evolution HORIBA Jobin Yvon A Raman microscope (Longmujeau, France) using a 633 nm He–Ne laser (Melles Griot, IDEX Optics and Photonics, Albuquerque, NM, USA) equipped with 1800 lines per 1 mm grating.

2.3 Rheological measurements

The rheological properties were measured with a stress-controlled rheometer (DHR 3, TA Instruments) using a parallel plate geometry. A 20 mm Peltier plate/ UV transparent plate was used as bottom plate and a smooth stainless steel 12 mm disk was used as top plate. The rheometer was equipped with a UV Source (OmniCure, Series 1500, 365 nm, 6 mW/cm^2) for illumination of the hydrogel samples in between the rheometer plates. Experiments were performed at room temperature (22-23°C). To avoid drying of the sample by evaporation during testing a solvent trap was used and the sample was sealed with silicone oil.

The 30 wt. % DA X hydrogels were prepared by pipetting 35 µL of a freshly prepared 30 wt. % DA X precursors solution on the rheometer plate, and allowing the gel to form between the plates (diameter 12 mm, gap 300 µm) during 10 min. The polymerization of the acrylate groups was initiated by exposure to 365 nm (6 mW/cm^2) through the UV transparent bottom plate. Strain sweeps were conducted from 0.001% to 1000% at a frequency of 1 Hz. In the strain amplitude sweep curves, a line was fit to the plateau region (linear) and the drop-off region (non-linear). The intersection is taken as the critical strain value (γ_y).[27][28] Fluidization strain (γ_F) was taken as the value at the intersection of G' and G'', i.e., at G' = G'').[28] The corresponding stress values were used as critical stress (τ_y) and fluidization stress (τ_F) values. The experimental conditions for the rheological experiments were taken from our previous work.[1]

2.4 Stress relaxation measurements

In the stress relaxation experiment, strains of 0.5, 1, 2, 5, 10, 15 and 30 % were applied to the same sample (DA 0, 50 and 100, n=3) for 300 s with a strain raise time of 0.2 s. To avoid cumulative stress buildup and shear history effects, the strain was reversed (negative strain, equivalent to the positive strain) after each run to reach rheometer stress = 0 Pa, and the next run was started after 10 min equilibration time.

In another experiment, a constant strain of 1% was applied to the sample (strain raise time 0.01 s) and the stress was monitored for 300 s. Each experiment was repeated three times.

The percentage of relaxation was defined as the drop in the relaxation modulus from the start (30 ms) to the end (300 s) of the experiment normalized by the starting relaxation modulus[29].

The relaxation curves were fitted to a linear combination of two stretched exponential or Kohlrausch–Williams–Watts (KWW) functions,[30]

$$G = G_0 \left\{ \left(A \times \exp\left[-\left(\frac{t}{\tau_1}\right)^{\beta_1}\right]\right) + (1 - A) \times \exp\left[-\left(\frac{t}{\tau_2}\right)^{\beta_2}\right] \right\} + G_e \qquad \text{.....(1)}$$

where G_0 is the relaxation modulus linearly extrapolated to zero time, τ_1 and τ_2 are the viscoelastic relaxation times for the two processes ($0 < \tau$), β_1 and β_2 are stretching exponents for the two processes ($0 < \beta \leq 1$) that reflect the width of the relaxation time distribution. The parameter A is the fractional contribution of the fast relaxation to the whole relaxation process ($0 < A$) and G_e is the equilibrium relaxation shear modulus.

2.5 Creep recovery measurements

A shear stress of 100 Pa was applied for 180 s to the hydrogel sample in the rheometer. The shear strain was monitored during this time (creep phase), and for a further 180 s after

removal of the shear stress (recovery phase). Creep ringing phenomenon was observed at short time scales (2 s) in the creep and recovery experiments.[31]

Creep deformation, γ_{creep}, was fitted to a four parameter Burgers model:[32][33][34]

$$\gamma_{creep} = \frac{\tau}{G_m} + \frac{\tau}{G_k}\left(1\text{-}\exp^{\frac{-t}{\lambda}}\right) + \frac{\tau}{\eta_m}t \qquad \text{.....(2)}$$

where, τ is the applied shear stress (fixed to 100 Pa), t denotes the time after loading, G_m denotes the shear modulus (or spring constant) of the spring and η_m denotes the viscosity of the dashpot in the Maxwell element. The parameter G_k denotes the shear modulus (or spring constant) and η_k denotes the viscosity of the dashpot in the Kelvin element and λ is the retardation time taken to produce 63.2% of the total deformation in the Kelvin element. The non-linear curve fit function of the OriginPro 9.1 software was used for the fitting and four parameters (G_m, G_k, η_m and τ) were defined. Creep ringing phenomenon was observed at short time scales. Therefore only data at $t > 2$ s were considered in the fitting process.[31]

Recovery data was fitted to a Weibull distribution function.[32][35]

$$\gamma_{rec} = \gamma_k \left\{\exp\left[-\left(\frac{t-t_0}{\eta_r}\right)^{\beta}\right]\right\} + \gamma_p \qquad \text{..... (3)}$$

where where γ_{rec} denotes the deformation after the instantaneous strain recovery, γ_k denotes the delayed viscoelastic strain recovery (Kelvin-Voigt element), η_r is the characteristic life parameter, t_0 is an induction time and β the shape factor. The stress is removed at time t_0 (180 s) and γ_p is the permanent irreversible strain. Ringing phenomenon was observed again at short time scales as in creep data. Therefore t_0 = 182 s was considered for the fitting.

2.6 Statistical Analyses

Non-linear curve fit function of the OriginPro 9.1 software was used for the fitting of the rheological curves. Concrete parameters used for the different types of analyses performed have been described in the sections and figure captions of the related experiments.

3 Results

The 30 wt. % Plu/PluDA hydrogels were prepared by mixing defined volumes of 30 wt. % solutions of Plu and PluDA polymers.[1] Hydrogels were named DA X**,** with X being the fraction of PluDA in the Plu/PluDA mixture, between 0 and 100 % (**Table 1**). In the following we describe first the rheological behavior of the physical DA X hydrogels, and of the physical and covalently crosslinked DA X hydrogels.

3.1 Rheological behavior of physical Plu and PluDA hydrogels

A 30 wt. % solutions of Pluronic F127 (Plu) in water form physical hydrogels at temperature >15.5°C.[1] At room temperature (22°C) and shear strain amplitudes (γ_0) below 1 %, the Plu (= DA 0) hydrogel behaves as a linear response viscoelastic solid (**Figure 1a**) with a strain amplitude independent shear modulus G' of 15.3 ± 1.6 kPa (**Figure 1b**) at $\omega/2\pi$ = 1 Hz. At higher strain amplitudes (γ_0 > 1%), Plu hydrogels show strain-induced yielding and gradual fluidization (**Figure 1a**). This behavior is characteristic of colloidal or granular hydrogels,[36] in which particles aggregate through reversible interparticle interactions to form an interconnected, percolated 3D network structure that yields when the applied stress exceeds the interparticle attractive forces.[27] The critical strain for yielding mainly depends on the particle content and the strength of the interparticle interactions including interparticle (electrostatic, hydrogen bonding, van der Waals, steric, depletion etc.) and hydrodynamic forces.[37]

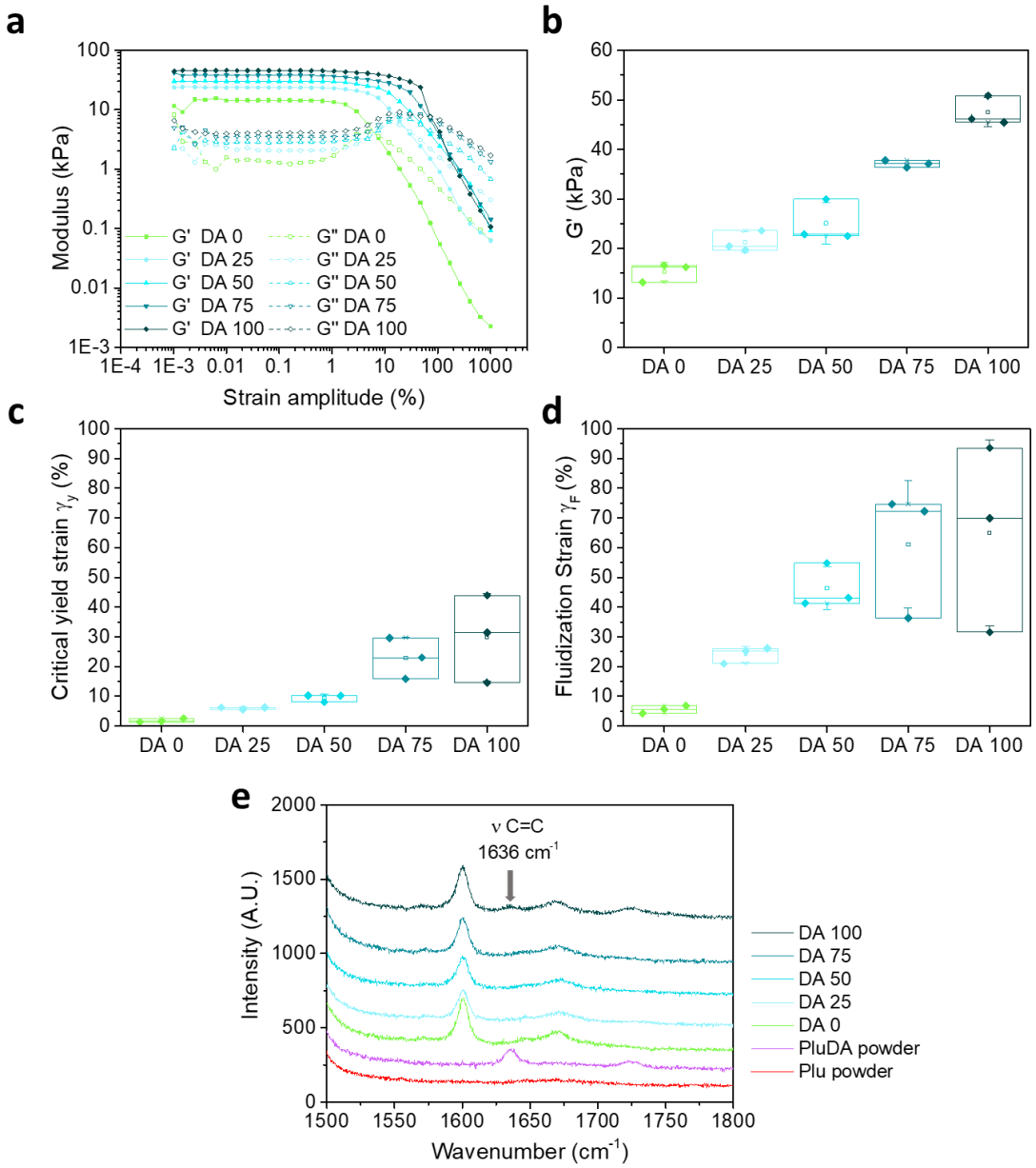

Figure 1. a) Representative strain amplitude sweeps of DA X hydrogels measured at a frequency of 1 Hz; **b)** G' values of DA X hydrogels from (a) at 0.1 % strain amplitude at a frequency of 1 Hz; **c)** Values of strain amplitude at critical yield point, γ_Y, and **d)** strain amplitude at fluidization point, γ_F, of DA X hydrogels as function of X obtained from the strain amplitude sweep experiment in **a**), (N = 3, box represents 25 and 75 percentile values and whiskers indicate standard deviation); **e)** Raman spectra (vertically shifted for clarity) of Plu and PluDA powders and DA X hydrogels. PluDA powder shows the C=C stretching mode (ν) at 1636 cm^{-1}. The band at 1600 cm^{-1} in DA X hdyrogels corresponds to the -OH bending mode of water molecules, which is absent in Plu and PluDA powders.

Table 1: Composition and mechanical parameters of DA X hydrogels. Note that the end-group functionalization degree of PluDA component is 70% and, therefore, the real fraction of covalent fixed chains differs for each composition and reaches 70% as maximum value in DA 100.

Hydrogel name (DA X)	Plu:PluDA ratio (mol %)	Ratio of diacrylated endgroups[1] (%)	Shear storage modulus[2] G' (kPa)	Strain amplitude at yield point[2] γ_Y (%)	Strain amplitude at fluidization[2] γ_F (%)	Critical stress[3] τ_Y (kPa)	Fluidization stress[4] τ_F (kPa)
DA 0	100 : 0	0	15.3 ± 1.9	1.8 ± 0.6	5.5 ± 1.3	0.2 ± 0.0	0.2 ± 0.0
DA 25	75 : 25	17.5	21.2 ± 2.1	6.0 ± 0.4	24.1 ± 2.8	0.9 ± 0.0	1.7 ± 0.0
DA 50	50 : 50	35	25.1 ± 4.2	9.5 ± 1.2	46.4 ± 7.3	1.7 ± 0.3	3.9 ± 0.2
DA 75	25 : 75	52.5	37.1 ± 0.7	22.8 ± 6.9	61.1 ± 21.4	5.2 ± 0.8	6.7 ± 0.6
DA 100	0 : 100	70	47.5 ± 2.9	30.0 ± 14.7	65.0 ± 31.3	8.3 ± 3.1	9.9 ± 0.9

[1] *calculated taking into account 70% end-group functionalization of PluDA*

[2] *from strain amplitude sweep, values at $\gamma_0 = 0.1$ % and frequency = 1 Hz (**Figure 1a**)*

[3] *corresponding stress values of γ_Y*

[4] *corresponding stress values of γ_F*

The 30 wt. % solutions of diacrylated Pluronic F127 (PluDA, 70 % end-group functionalization) also form physical hydrogels at a slightly lower temperature of 14°C.[1] The substitution of the terminal –OH groups by less polar acrylic functionalities in the outer surface of the PEO shell of Pluronic micelles enhances micellar aggregation and gel formation.[12] The resulting physical PluDA hydrogel shows a similar G' in the linear viscoelastic region (**Figure S1a**) and a two-fold higher critical strain amplitude for yielding in the strain sweep experiment (**Figure S1b**) compared to the Plu hydrogel, confirming stronger inter-micellar interactions in the gels with acrylate end-groups.

The strain sweep curves of the physical Plu and PluDA hydrogels show an overshoot in G'' at intermediate strain amplitudes between the linear viscoelastic and the fluidization regions. This overshoot is referred to as the Payne effect and is related to yielding as a gradual

transition that occurs while the deformation increases.[38] Strain-dependent breakdown of the internal structure, length scale-dependent rearrangements or forced stress relaxation are believed to contribute to the overshoot of G'' as a function of applied strain amplitude.[38]

3.2 Rheological behavior of physically vs. physically and covalently crosslinked PluDA hydrogel

Covalently crosslinked PluDA (=DA100) hydrogels were prepared from 30 wt. % PluDA solutions containing 0.2 wt. % Irgacure 2959. The solution was left to form a physical gel between the rheometer plates, and it was covalently crosslinked subsequently by exposure to 365 nm light through the UV transparent bottom plate. The degree of conversion of the acrylate groups after polymerization was evaluated by Raman spectroscopy. The characteristic band for the stretching of the C=C bond, observed at 1635 cm^{-1} in the spectrum of PluDA powder, diminished in Plu powder and in the PluDA hydrogel after UV irradiation (**Figure 1e**). This indicates nearly full conversion of the acrylate groups in the photo-crosslinking step.

The polymerization of the acrylate groups influenced the rheological response of the PluDA hydrogel. The covalently crosslinked hydrogel showed a broader linear viscoelastic range than the exclusively physically crosslinked PluDA, with strain amplitude independent moduli up to $\gamma_0 = 10\%$ (**Figure S1a**). At higher strain amplitudes, a continuous drop in G' was observed. This strain induced yielding and gradual fluidization suggests that the micellar network in the covalent crosslinked PluDA hydrogel can undergo major reorganization and stress dissipation and stress release in spite of 70% of the endgroups of the polymeric chains being covalently crosslinked. This behavior can be understood considering that acrylate groups at the PluDA chain terminals can form inter- and intra-micellar crosslinks during the

photoinduced polymerization reaction.[12] Micellar clusters which are covalently crosslinked are expected to contribute to the elasticity of the hydrogel and be the reason for the higher G' and higher critical yielding strain of the covalently crosslinked PluDA hydrogel compared to the physically crosslinked PluDA hydrogel (30 ± 14.7 v*s.* 4.2 ± 0.8 %, **Figure 1c, S1b**). Intra-micellar crosslinks stabilize the micelles and form loops in the chains. These crosslinks do not interfere with the inherent ability of physical micellar aggregates to flow above the critical strain. Note that the average residence time of a Pluronic molecule in a physical micellar aggregate has been estimated to be several hours.[39] Therefore, crosslinking during photopolymerization (1 min time scale) can mainly occur between chain ends located in close proximity. The observed strain-induced yielding and fluidization (**Figure 1d**) above a critical yield stress in our PluDA hydrogels suggests that a significant fraction of the covalent crosslinks are intra-micellar. This has been previously suggested by other authors based on gel permeation chromatography (GPC) and light scattering analysis of the sol phase after crosslinking and cooling below the transition temperature.[12]

3.3 Rheological behavior of covalently crosslinked Plu/PluDA hydrogels with variable PluDA content

We analysed the rheological response of Plu/PluDA covalent hydrogels as a function of the degree of covalent crosslinking. Near full conversion after the photo-crosslinking step was confirmed by Raman spectroscopy (**Figure 1e**).

Covalently crosslinked DA X hydrogels showed an increasing trend of G', γ_Y and γ_F values from Plu (=DA 0) to PluDA (=DA 100) hydrogels. The strain amplitude sweeps showed both a linear viscoelastic and a fluidization region. The storage modulus G' at 0.1 % strain amplitude increased from 15.3 ± 1.8 to 47.5 ± 2.9 kPa as the PluDA content increased from 0 to 100 % (**Figure 1c**). The critical strain for yielding at 1 Hz, γ_y, also increased from 1.7 ± 0.4 % to 29.7 ±

15.2 % (**Figure 1d, Table 1**) from DA 0 to DA 100. The strain amplitude needed to reach the fluidization point (crossover of G'' and G', as opposite to gelation point), γ_F, increased from 5.5 ± 1.2 % to 65.0 ± 31.3 % (**Figure 1e**) and the corresponding stress values at the fluidization point ranged from 0.2 ± 0.0 kPa to 9.9 ± 0.9 kPa (**Figure S2, Table 1**). The increase in the density of covalent links between neighboring micelles (inter-micellar) with increasing X hinders the viscous deformation of the hydrogel and higher mechanical stability and elasticity under the applied strain.

3.4 Stress relaxation of DA X hydrogels

Figure 2a-c shows the stress induced in DA 0, DA 50 and DA 100 hydrogels during a stress relaxation experiment with step-strain increase from 0.5 to 30 % (300 s) and strain raise time of 200 ms. The stress relaxation curves normalized by the maximum stress values attained during the 200 ms strain raise are also shown. In physical DA 0 hydrogels, the maximum induced stress increased from 78 ± 17 Pa to 231 ± 55 Pa with increasing applied strain from 0.5 to 5 %, and it plateaued for larger shear deformations (**Figure 2d**). In contrast, the maximum induced stress in covalently crosslinked DA 100 increased linearly with the strain up to 15 % and reached values up to 5708 ± 246 Pa (**Figure 2d**), denoting a primarily elastic behavior within this strain range. DA 50 showed an intermediate behavior. These differences are in agreement with the observations from the strain sweep experiment (**Figure 1c**), where γ_Y of physical DA 0 hydrogel was 1.8 ± 0.6% while that for covalently crosslinked DA 100 hydrogel was 30.0 ± 14.7 %.

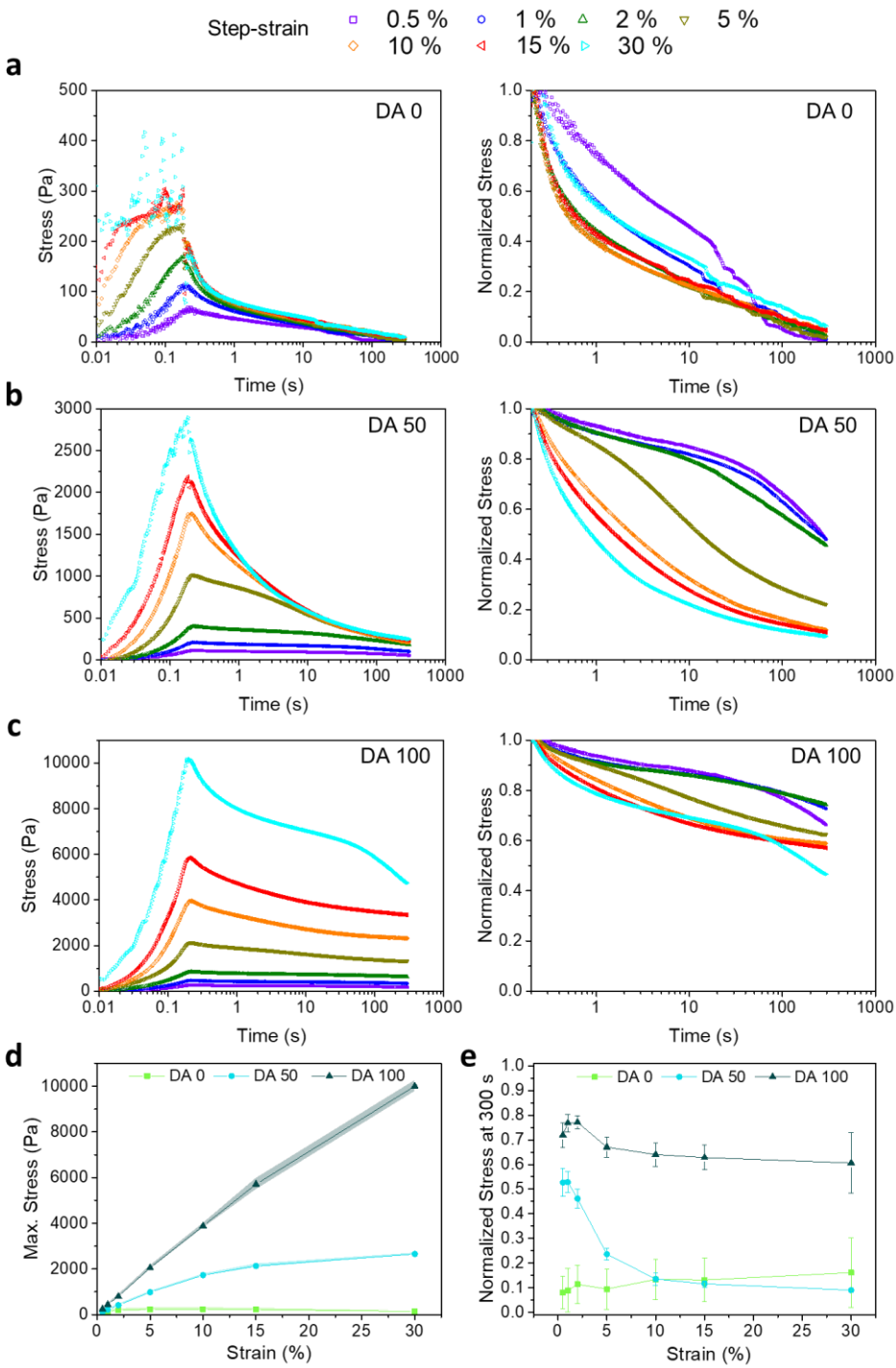

Figure 2: Representative step-strain stress relaxation curves as a function of increasing applied strain values from 0.5 to 30 % on **a)** DA 0, **b)** DA 50 and **c)** DA 100 hydrogels (left) with their corresponding normalized stress values (right, normalized with maximum stress values at 200 ms strain raise time); **d)** Mean maximum stress values at 200 ms (strain raise time) and **e)** Normalized stress values at the end of the stress relaxation test (300 s). Error bars indicate standard deviation, N=2 for DA 0 and DA 50 at 30 % applied strain, N=3 for all the rest.

The strain-dependent stress relaxation curves of DA X hydrogels were also dependent on the amount of X (**Figure 2a**). Whereas DA 0 was able to relax the induced step shear stress almost completely within 300 s at all strain values, DA 100 retained at least 60% of the stress, in agreement with its elastic nature (**Figure 2e**). DA 50 showed an intermediate behavior with up to 50% relaxation for shear strains <2%, whereas it relaxed >70% for larger strain values. For all hydrogels, the step shear stress was dissipated faster at higher strains, when the γ_F range was reached (**Figure 2e**).

The comparative relaxation behavior of DA X hydrogels (for X = 0, 25, 50, 75 and 100) at 1 % strain, i.e., within the linear viscoelastic regime, is shown in **Figure 3**. The shape of the curves indicates that stress is dissipated by two different relaxations processes with different time scales: a fast first one (<1 s) and a slower second one (>1 min). To analyze the relaxation mechanisms behind the two processes, the stress relaxation curves were fitted to a linear combination of two stretched exponential functions **(Eq. 1)**[30]:

$$G = G_0 \left\{ \left(A \times \exp\left[-\left(\frac{t}{\tau_1}\right)^{\beta_1}\right]\right) + (1 - A) \times \exp\left[-\left(\frac{t}{\tau_2}\right)^{\beta_2}\right] \right\} + G_e \qquad \text{.....(1)}$$

where G_0 is the relaxation modulus linearly extrapolated to zero time, τ_1 and τ_2 are the viscoelastic relaxation times for the two processes, β_1 and β_2 are stretching exponents for the two processes ($0 < \beta \leq 1$) that reflect the width of the relaxation time distribution. The parameter A is the fractional contribution of the fast relaxation to the whole relaxation process ($0 < A$) and G_e is the equilibrium relaxation shear modulus. This function fitted well with the experimental data with $r^2 > 0.99$ (**Figure 3c**). The values of G_0, G_e, A, τ_1, τ_2, β_1, and β_2 and are represented in **Figure 3 d-j** as a function of the hydrogel composition. The two relaxation times τ_1 (<1 s) and τ_2 (>1 min) differed in more than two orders of magnitude and showed an opposite dependence on the degree of the covalent crosslinking of the hydrogels.

τ_1 decreased from 0.25 s to 0.01 s as X increased from 0 to 100 (**Figure 3g**), i.e. the fast relaxation became faster as the covalent crosslinking degree increased. The relative contribution of this relaxation mode to stress dissipation (A parameter, **Figure 3f**) increased with the covalent crosslinking of the hydrogel. The shape parameter β_1, which reflects the width of the relaxation time distribution, did not show significant changes with the hydrogel composition and is around 0.3-0.4 (**Figure 3g**) reflecting a 2-3 decade wide relaxation distribution. The relaxation process at longer time scales became slower in hydrogels with increasing covalent crosslinking (mean τ_2 increased from nearly 100 s to 560 s for DA 0 to DA 100, **Figure 3h**) and the strength of this relaxation decreased with X. The possible mechanisms behind these relaxations are weighed up further in the discussion section.

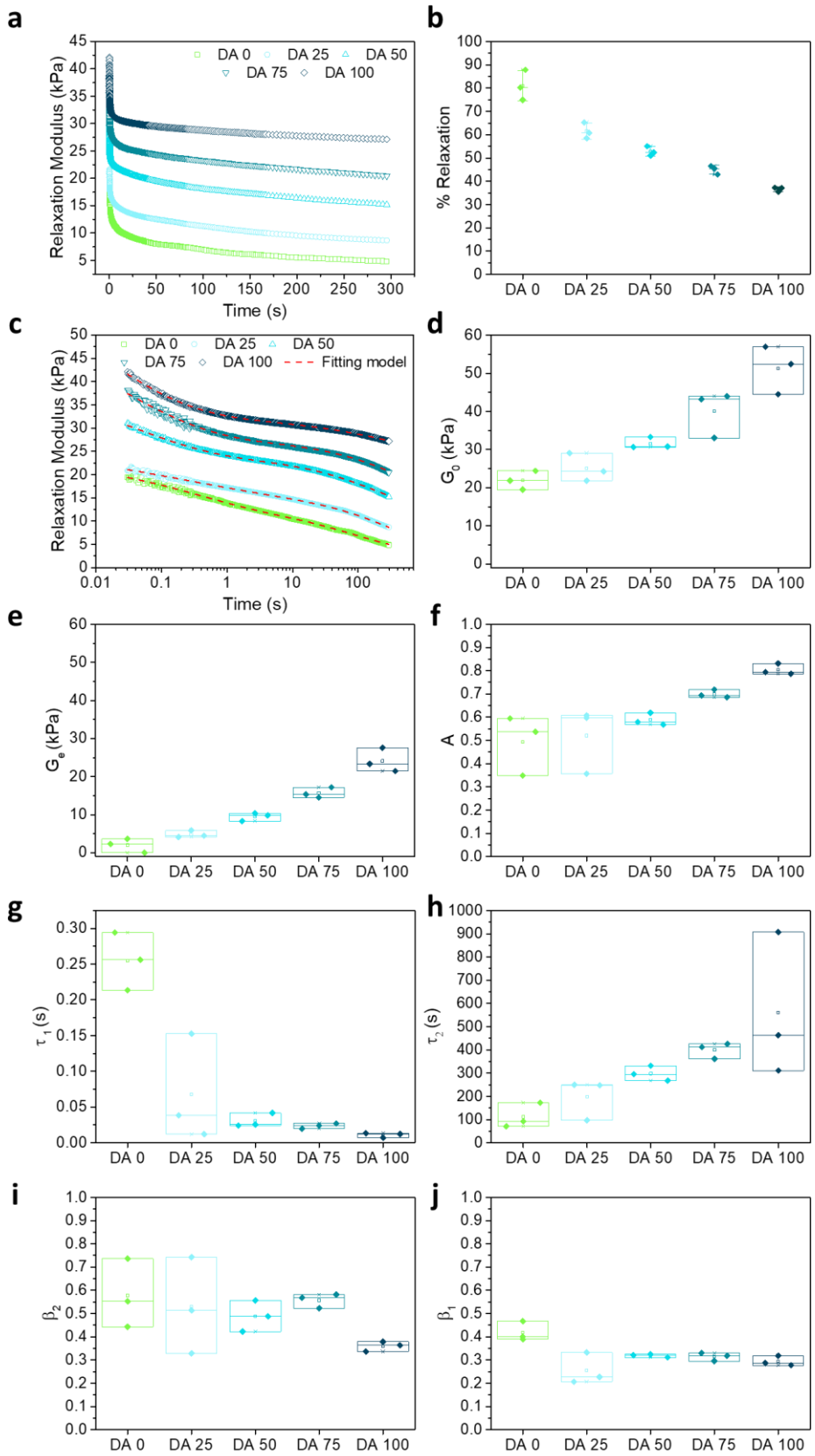

Figure 3: a) Representative stress relaxation curves of crosslinked DA X hydrogels at a constant applied strain of 1 %. **b)** Calculated normalized drop of relaxation modulus in DA X

hydrogels from experiment in a) at time t = 300 s (see details in experimental section). **c)** Stress relaxation curves from a) represented on a logarithmic scale and the fits with a double stretched exponential function (red dashed lines). Data below 30 ms were not considered for the fitting since this time was required by the equipment to reach a stable strain value of 1 %; **d)** G_0 values as function of X that were extrapolated linearly from stress relaxation curves in a) to time zero. **e-j)** Fitted parameters as a function of X: **e)** G_e; **f)** A (fractional contribution of relaxation 1, fast relaxation process); **g)** τ_1 ; **h)** τ_2 ; **i)** β_1 and **j)** β_2. The experimental curves of three consecutive measurements are shown in **Figure S3**. All measurements were performed at room temperature. N = 3, box represents 25 and 75 percentile values and whiskers indicate standard deviation.

3.5 Creep-recovery of DA X hydrogels

Figure 4a shows a creep-recovery experiment with DA X hydrogels at a constant stress of 100 Pa. In DA 25-75 hydrogels an instantaneous deformation was observed, followed by a slower deformation (creep). The instantaneous deformation was more pronounced in hydrogels with higher covalent crosslinking, while the creep process was more pronounced in hydrogels with lower PluDA concentration. DA 100 reached the plateau right after the initial deformation. DA 0 was the farthest from reaching a plateau deformation value during the 180 s of creep. When the 100 Pa stress ceased, an instantaneous and a time-dependent strain recovery was observed for all samples. DA 50-100 almost instantaneously fully recovered to their initial state, which is in agreement with their predominant elastic character as consequence of the covalent crosslinks. In comparison to that, DA25 and DA0 retained a residual deformation (**Figure 4a**), in agreement with their predominant physical gel character.

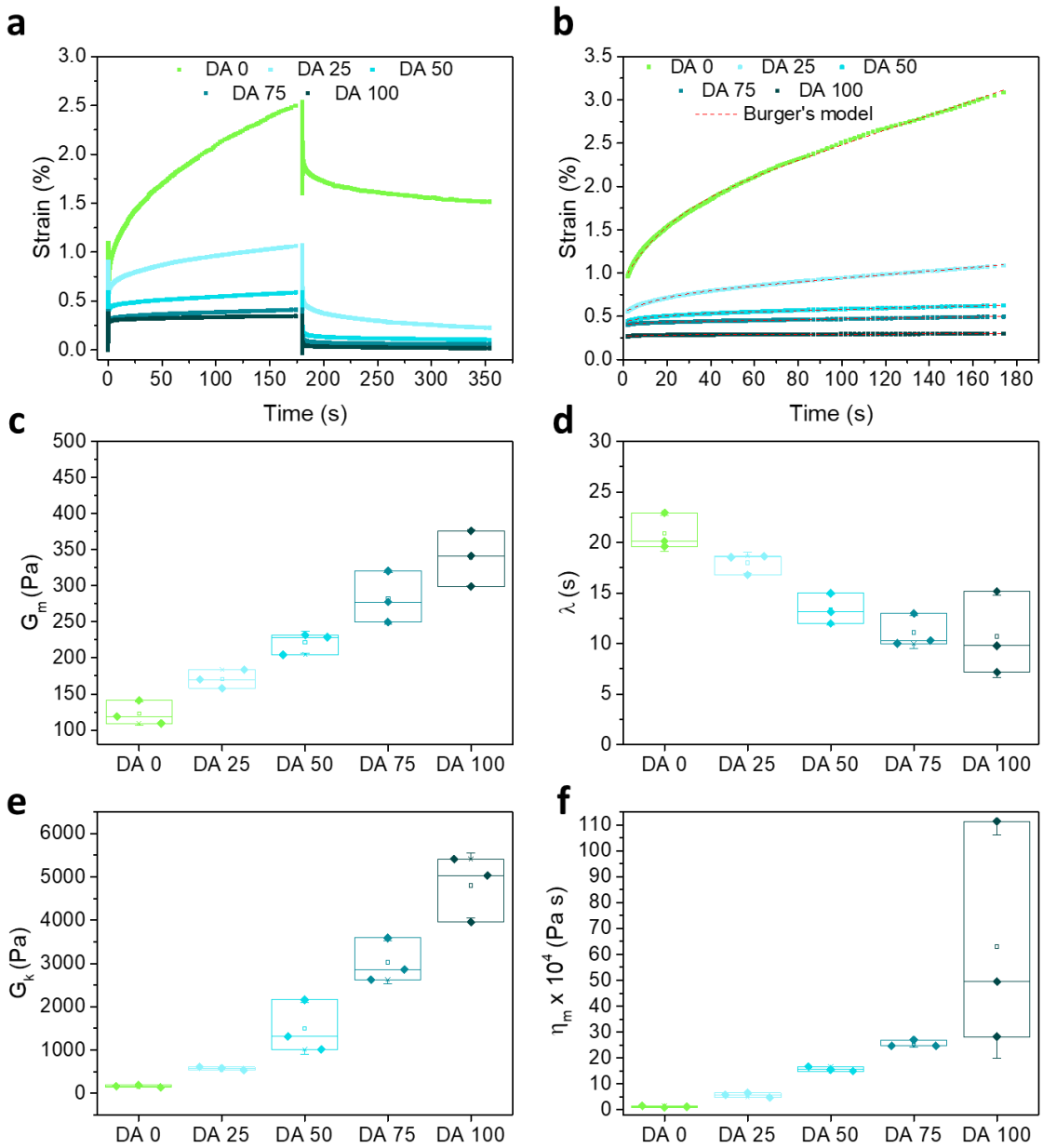

Figure 4: **a)** Representative creep/recovery curves of DA X hydrogels at an applied stress of 100 Pa for 180 s. The strain was monitored during stress application and also during the recovery phase for additional 180 s. **Figures S4 and S5** show all experimental curves. **b)** Creep curves and fittings to the Burgers model (Eq. 3, red dotted lines), **c-f)** parameters of the Burgers fitting represented as a function of X. G_m and η_m denote the spring constant of the spring and the viscosity of the dashpot in the Maxwell element, G_k is the spring constant of the dashpot in the Kelvin element and λ is the retardation time. N = 3, box represents 25 and 75 percentile values and whiskers indicate standard deviation.

The creep curves were fitted to a four-elements Burgers model[32][33][34], consisting of Maxwell and Kelvin-Voigt elements.[35][40] In this model, the strain during creep, γ_{creep} , is expressed as:

$$\gamma_{creep} = \frac{\tau}{G_m} + \frac{\tau}{G_k}\left(1-e^{\frac{-t}{\lambda}}\right) + \frac{\tau}{\eta_m}t \quad \ldots\ldots(2)$$

where τ is the applied shear stress (100 Pa), t denotes the time after loading, G_m denotes the spring constant of the spring , η_m denotes the viscosity of the dashpot in the Maxwell element, G_k is the spring constant of the dashpot in the Kelvin element, and λ is the retardation time (η_k/G_k) needed to achieve 63.2% of the total deformation in the Kelvin unit (where η_k is the viscosity of the dashpot in the Kelvin element). The Burgers model fit was applied to the experimental data (red dashed lines in **Figure 3c**) and obtained fitting parameters as function of the hydrogel composition are represented in **Figure 3d-j**. The elastic constants G_m and G_k increased in DA X hydrogels with increasing X, and therefore an increased elasticity is observed due to a higher number of crosslinks. The reorganization of covalently linked micelles and clusters requires additional work, which causes an increment in the opposition to deformation. This higher resistance capacity contributes to elasticity. In the Burgers model, the retardation time λ is connected to the viscoelastic solid material behavior. In the micellar hydrogel model described before, the viscoelastic response is expected to depend on the intermolecular forces between micelles connected by inter-micellar covalent bonds. The shorter retardation times observed with increasing X indicate that the covalent connection between the micelles accelerates the sliding of micelles and the deformation of the hydrogel. Furthermore, η_m increases with X and reflects the increasing dissipative resistance, and thus lesser deformation due to the viscous component. We associate this with sliding of micelles and clusters connected by physical interactions.

The recovery part of the creep experiment was fitted using a Weibull distribution equation that is a modification and extension of a simple exponential relaxation. The strain $\gamma_{recovery}$ is expressed as[32]:

$$\gamma_{recovery} = \gamma_k \{\exp\left[-\left(\frac{t-t_0}{\eta_r}\right)^{\beta}\right]\} + \gamma_p \qquad \text{..... (3)}$$

where γ_k denotes the delayed viscoelastic strain recovery (Kelvin-Voigt element), η_r is the characteristic life parameter, β the shape factor, t_0 the time when the stress is removed, and γ_p the permanent irreversible strain. The Weibull equation fitted the experimental data (**Figure 5a**). The delayed viscoelastic strain recovery γ_k decreased with increasing covalent crosslinking in DA X hydrogels, reflecting that the presence of permanent crosslinks hinders viscoelastic deformation. The permanent irreversible strain γ_p was 10 times higher for DA 0 than for the other hydrogels as consequence of the absence of covalent bonds that provide elasticity.

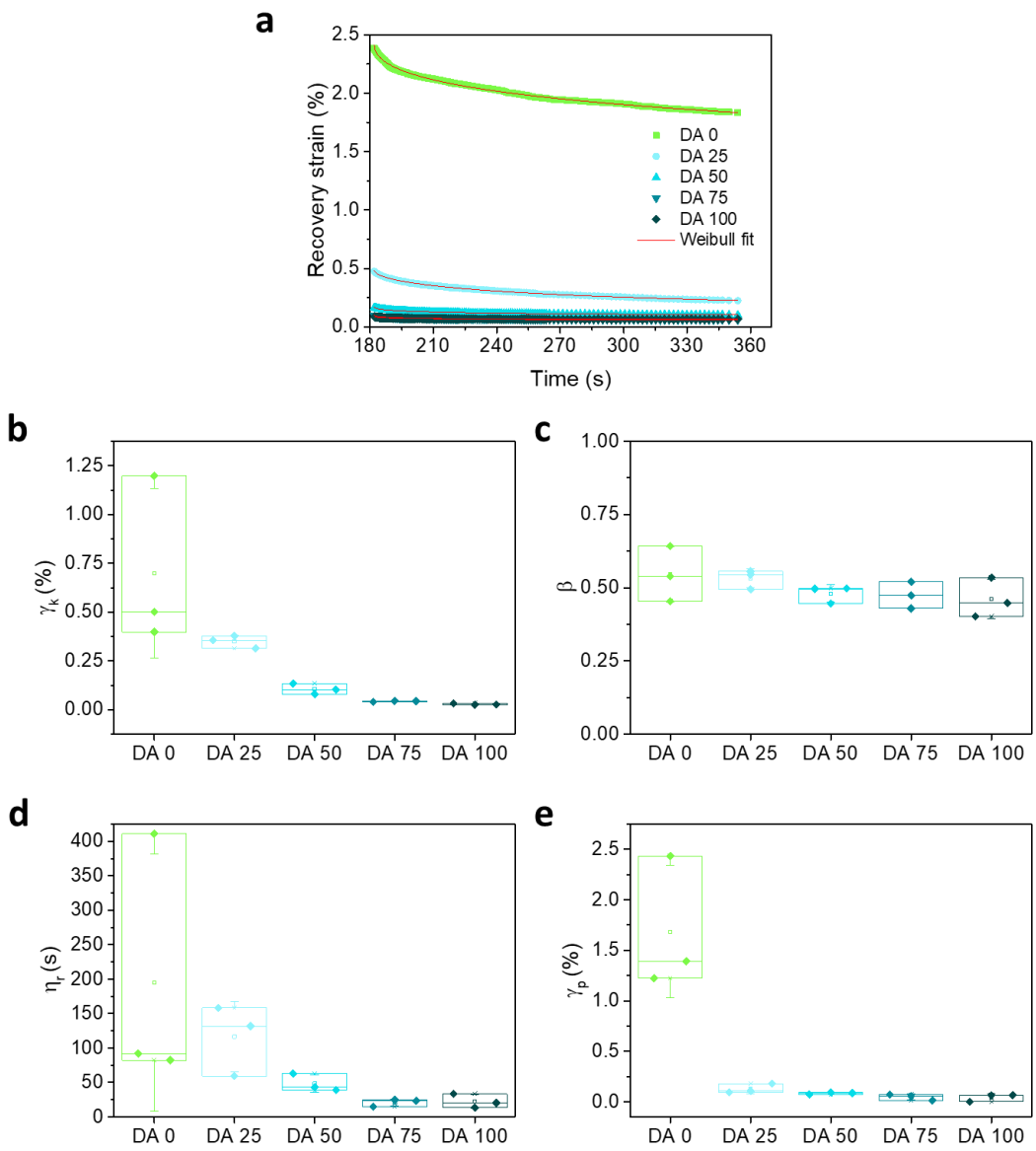

Figure 5: **a)** Recovery curves including fittings to the Weibull distribution function and **b-e)** parameters of the Weibull fitting as function of DAX composition. N = 3, box represents 25 and 75 percentile values and whiskers indicate standard deviation.

The elastic recovery corresponds to the instantaneous recovered deformation, that is, the Maxwell spring. $\gamma_{maxwell\ spring}$ was calculated as:

$$\gamma_{maxwell\ spring} = \gamma_{ms} = \gamma_{maximum} - (\gamma_k + \gamma_p) \quad \text{.....(4)}$$

where $\gamma_{maximum}$ is the strain at the end of the creep test. The elastic as well as the viscoelastic and plastic contributions to the deformation extracted from the Weibull model are

represented in **Figure 6**.[32] At an applied stress of 100 Pa, hydrogels DA 25-100 showed increasing elastic and decreasing viscoelastic responses with increasing covalent crosslinking, and a small plastic response with little dependence on X. DA 0 hydrogels showed a strong plastic response and a comparatively much lower elastic and viscoelastic contributions.

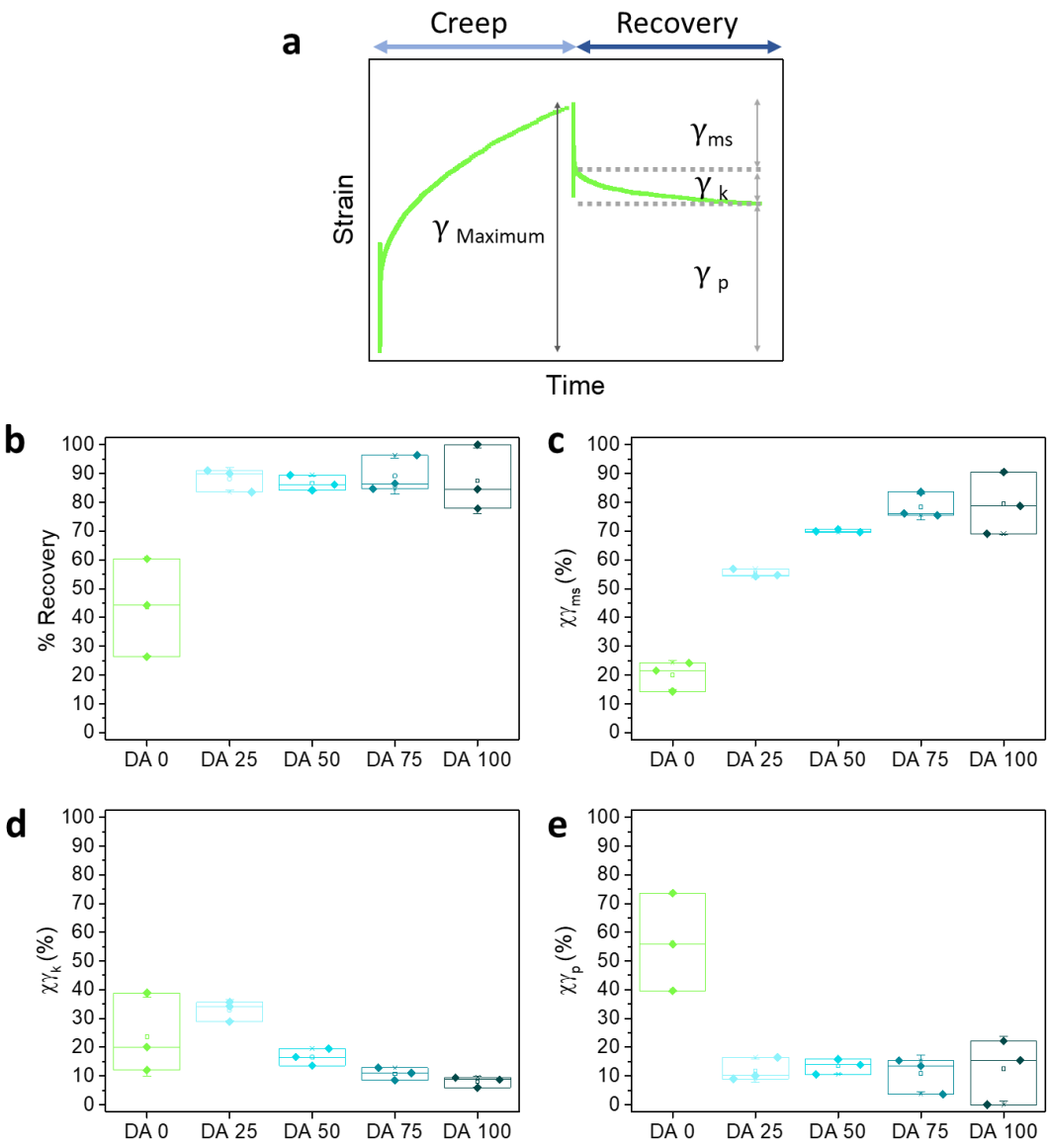

Figure 6: a) Elastic, viscoelastic and plastic contributions obtained from the creep-recovery experiment. The curve corresponds to DA 0 at an applied stress of 100 Pa; **b)** Recovery (%) calculated from recovery curves at 180 s after 100 Pa applied stress; **c-e)** Contributions of elastic, **d)** viscoelastic and **e)** plastic deformation. N = 3, box represents 25 and 75 percentile values and whiskers indicate standard deviation.

3.6 Attempts to correlate the observed rheological response of DA X hydrogels and bacterial growth from previous reports[1]

Our previous studies of *E. coli* within 30 wt% DA X hydrogels showed that the degree of covalent crosslinking of the hydrogel affected the growth of embedded *E. coli* bacteria colonies.[1] The maximum volume achieved by a growing colony decreased with increasing DA X content. In **Figure 7** we display the normalized values of the colony volume (data from our previous work[1]), of the storage modulus (from **Figure 1c**) and the critical stress for fluidization τ_F (from **Figure S2c**) corresponding to DA X hydrogels as function of X. The three parameters decrease (colony volume) or increase (G' and τ_F) with X in DA0-75 hydrogels. The colony volume in DA 100 is similar as in DA 75, suggesting that the mechanical differences between these two hydrogels are out of the mechanosensing capacity of the bacteria colonies. The elastic contribution to deformation $X\gamma_{ms}$ (**Figure 6c**) in our creep-recovery experiments was similar for DA 75 and DA 100 and correlated inversely with the trend of colony volume, suggesting that this could also be a relevant mechanical parameter to dictate bacteria behavior inside the hydrogels.

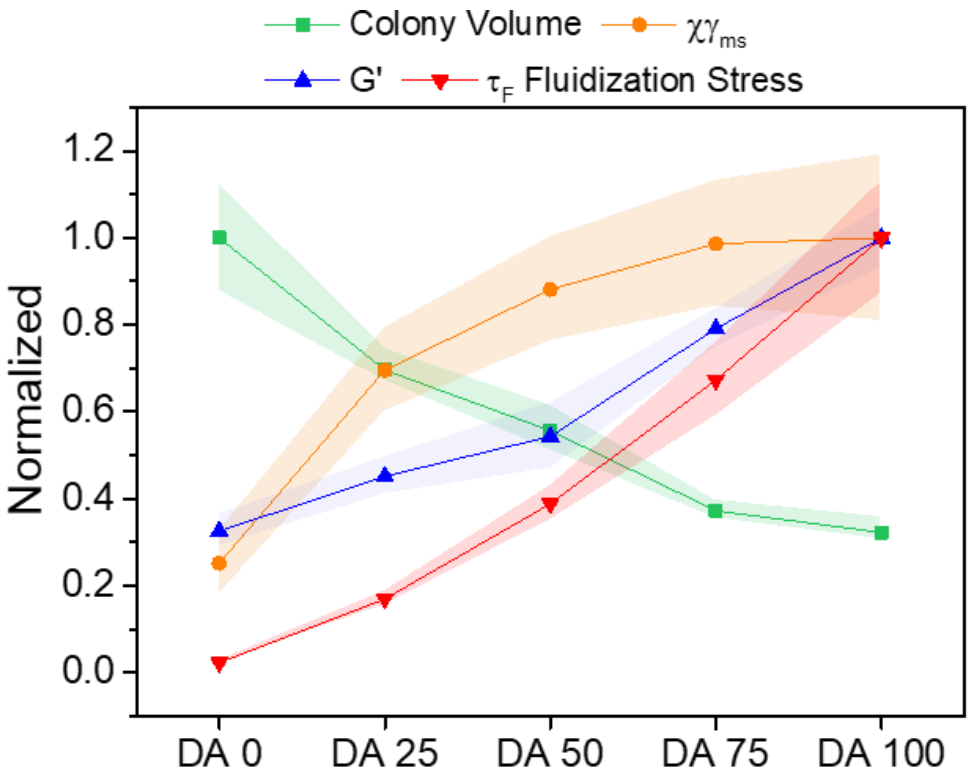

Figure 7: Comparative plot of normalized mechanical parameters and bacteria growth volume as function of DA X composition. The represented normalized parameters are: Colony volume (95th percentile volumes of colonies after 24 h growth)[1], the elastic contribution to deformation Xγ_{ms} (maxwell spring) in creep-recovery experiments (applied stress of 100 Pa), shear storage modulus G' (at 1 Hz) and Fluidization stress τ_F. The values were normalized with respect to the highest value in each category. The symbols and shaded regions of the normalized colony volume data indicate 95 ± 2 percentile value range, for all other data the symbols and shaded regions indicate mean ± SD.

4 Discussion

Micellar DA X hydrogels are considered granular gels.[41][42] Our rheological observations agree with this picture. In general, the internal structure of granular gels depends on the particle volume fraction and the strength of inter-particle interactions.[43] At high particle volume fractions and weak interaction forces, gelation occurs as a consequence of the dynamical arrest of a phase separation process.[44] In the particle-rich domains, particles

aggregate and form clusters that grow until their dynamics is arrested within the 3D network.[45] Clusters act as rigid, load bearing units and have been postulated to be the origin of elasticity in colloidal gel networks. The reversibility of the interactions between particles allows for shear-induced rearrangement of the aggregates and particles by breaking reversible bonds. As a consequence, granular hydrogels show shear thinning behavior. The observed behavior of physical Pluronic hydrogels is in agreement with this picture. The inter-micellar covalent bonds introduced after physical gelation in DA X hydrogels reinforce the stability of the clusters and contribute to a stronger elastic character of the material.[42]

Previous literature discussed the behavior of Pluronic F127 hydrogels under shear.[17][46] Pluronic micelles are considered hard spheres and their regular aggregates can undergo a first order phase transitions (analog melting, recrystallization) or reorientation as function of shear conditions (shear stress, rate or direction).[17][46] Inter-micellar covalent bonds in DA X hydrogels internally stabilize micellar clusters and substantially affect such rearrangement mechanisms and underlying kinetics. We expect that the time scale of these rearrangements relates to the observed experimental time scales for the observed stress relaxation. Our fitting method for the stress relaxation curves of DA X hydrogels indicated two different relaxation processes with relaxation times τ_1 (<1 s) and τ_2 (>1 min) that depend on DA content. The fast relaxation process became faster and more prominent with increasing covalent crosslinking. We associate this relaxation to local, structural rearrangements at macroscopic, network scale which require cooperative motion of micelles.[47][48] In contrast, the slow relaxation process could be associated to relaxation modes at microscopic scale, such as the breaking of physical bonds between micelles within clusters, which becomes slower with increasing number of covalent crosslinks.[47][49] A recent article has studied the deformation mechanisms of 24 wt% PluDA hydrogel in an ionic liquid using

rheology and SANS.[50] The authors highlighted the possible contribution of free inter-micellar PluDA chains to elasticity by forming covalent inter-micellar bridges. Under tensile stress, the bridging chains would store mechanical energy during stretching and pull micelles back into their original positions after deformation. Although this model could explain our results, the range of stress applied was three orders of magnitude larger than the shear stress applied in our experiments and, therefore, the deformation mechanisms might differ.

The mechanical properties DA X gels in our work can regulate the growth of embedded bacteria according to our previous studies,[1] though the mechanism behind remains to be elucidated. Bacteria exert forces on the surrounding matrix while growing as consequence of their internal turgor pressure. This turgor pressure is characteristic for the bacteria species and is ranged between 30 and 300 kPa for *E. coli*.[10][51] The growth rate of *E. coli* in suspension and in the presence of nutrients is >20 minutes. According to our rheological results (**Figure 1a and S2**), a hypothetical stress of 10 kPa at a time scale of 20 minutes applied by growing *E. coli* to a surrounding DA X matrix would deform the hydrogel beyond the yield point. Therefore, the observed correlation in our studies between colony volume and the fluidization stress seems reasonable as a first interpretation. Additional studies and multiparametric models are needed to understand the underlying principles behind the dependence of bacteria growth and the mechanical properties of the confining space.

5 Conclusions

In this article, we present the rheological behavior of Plu/PluDA hydrogels with compositions relevant for embedding and culturing bacteria. We quantified the elastic, viscoelastic and plastic responses of DA X hydrogels with varying degree of covalent crosslinking. We attempted to correlate the mechanical parameters of the network with bacteria growth and could be used to predict the dynamics of a bacteria population embedded in Pluronic

hydrogels. The results confirm the correlation between bacteria growth and the mechanical response of the hydrogel, but we still lack a constitutive model with predictive potential. Additional studies with other shear strains and eventually other materials are needed for this step.

Embedded bacteria in hydrogel matrices are of relevance for biotechnological production and also for the developing field of engineered living materials. Being able to regulate bacteria growth in these application fields is of relevance to maximize production or to minimize risks associated to outgrowth of the organisms. Physical confinement of an expanding bacteria colony and the mechanical resistance of the environment to the colony growth are also proven to be important factors in triggering biofilm development, also in infection scenarios.[52] The results from the current and future work provide correlations between material parameters and cell responses in model encapsulated systems that could help to understand the natural cases.

Acknowledgements

The authors acknowledge support from the Deutsche Forschungsgemeinschaft (Collaborative Research Centre, SFB 1027) and the Leibniz Science Campus on Living Therapeutic Materials, LifeMat. The authors thank Lea Fischer for useful feedback.

Declaration of competing interest

The authors declare that they have no known competing financial interests or personal relationships that could have appeared to influence the work reported in this paper.

References

[1] S. Bhusari, S. Sankaran, A. del Campo, Regulating bacterial behavior within hydrogels of tunable viscoelasticity, Advanced Science. 2106026 (2022) 1–10. https://doi.org/10.1002/advs.202106026.

[2] M. Rizwan, A.E.G. Baker, M.S. Shoichet, Designing Hydrogels for 3D Cell Culture Using Dynamic Covalent Crosslinking, Advanced Healthcare Materials. 10 (2021) 2100234. https://doi.org/10.1002/adhm.202100234.

[3] X. Liu, M.E. Inda, Y. Lai, T.K. Lu, X. Zhao, Engineered Living Hydrogels, Advanced Materials. 34 (2022) 1–22. https://doi.org/10.1002/adma.202201326.

[4] D. Indana, P. Agarwal, N. Bhutani, O. Chaudhuri, Viscoelasticity and Adhesion Signaling in Biomaterials Control Human Pluripotent Stem Cell Morphogenesis in 3D Culture, Advanced Materials. 33 (2021) 2101966. https://doi.org/10.1002/adma.202101966.

[5] X. Liu, H. Yuk, S. Lin, G.A. Parada, T.C. Tang, E. Tham, C. de la Fuente-Nunez, T.K. Lu, X. Zhao, 3D Printing of Living Responsive Materials and Devices, Advanced Materials. 30 (2018) 1704821. https://doi.org/10.1002/adma.201704821.

[6] T.G. Johnston, S.F. Yuan, J.M. Wagner, X. Yi, A. Saha, P. Smith, A. Nelson, H.S. Alper, Compartmentalized microbes and co-cultures in hydrogels for on-demand bioproduction and preservation, Nature Communications. 11 (2020) 563. https://doi.org/10.1038/s41467-020-14371-4.

[7] T. Butelmann, H. Priks, Z. Parent, T.G. Johnston, T. Tamm, A. Nelson, P.J. Lahtvee, R. Kumar, Metabolism Control in 3D-Printed Living Materials Improves Fermentation, ACS Applied Bio Materials. 4 (2021) 7195−7203. https://doi.org/10.1021/acsabm.1c00754.

[8] A. Saha, T.G. Johnston, R.T. Shafranek, C.J. Goodman, J.G. Zalatan, D.W. Storti, M.A. Ganter, A. Nelson, Additive Manufacturing of Catalytically Active Living Materials, ACS Applied Materials and Interfaces. 10 (2018) 13373–13380. https://doi.org/10.1021/acsami.8b02719.

[9] H.H. Tuson, G.K. Auer, L.D. Renner, M. Hasebe, C. Tropini, M. Salick, W.C. Crone, A. Gopinathan, K.C. Huang, D.B. Weibel, Measuring the stiffness of bacterial cells from growth rates in hydrogels of tunable elasticity, Molecular Microbiology. 84 (2012) 874–891. https://doi.org/10.1111/j.1365-2958.2012.08063.x.

[10] Y.F. Dufrêne, A. Persat, Mechanomicrobiology: how bacteria sense and respond to forces, Nature Reviews Microbiology. 18 (2020) 227–240.

https://doi.org/10.1038/s41579-019-0314-2.

[11] D. Attwood, The micellar properties of the poly (oxyethylene) -poly (oxypropylene) copolymer Pluronic F127 in water and electrolyte solution, International Journal of Pharmaceutics. 26 (1985) 25–33.

[12] M. Di Biase, P. De Leonardis, V. Castelletto, I.W. Hamley, B. Derby, N. Tirelli, Photopolymerization of Pluronic F127 diacrylate: A colloid-templated polymerization, Soft Matter. 7 (2011) 4928–4937. https://doi.org/10.1039/c1sm05095h.

[13] R. Basak, R. Bandyopadhyay, Encapsulation of hydrophobic drugs in pluronic F127 micelles: Effects of drug hydrophobicity, solution temperature, and pH, Langmuir. 29 (2013) 4350–4356. https://doi.org/10.1021/la304836e.

[14] P. Prasanthan, N. Kishore, Self-assemblies of pluronic micelles in partitioning of anticancer drugs and effectiveness of this system towards target protein, RSC Advances. 11 (2021) 22057–22069. https://doi.org/10.1039/d1ra03770f.

[15] Q. Gao, Q. Liang, F. Yu, J. Xu, Q. Zhao, B. Sun, Synthesis and characterization of novel amphiphilic copolymer stearic acid-coupled F127 nanoparticles for nano-technology based drug delivery system, Colloids and Surfaces B: Biointerfaces. 88 (2011) 741–748. https://doi.org/10.1016/j.colsurfb.2011.08.010.

[16] J. Dey, S. Kumar, S. Nath, R. Ganguly, V.K. Aswal, K. Ismail, Additive induced core and corona specific dehydration and ensuing growth and interaction of Pluronic F127 micelles, Journal of Colloid and Interface Science. 415 (2014) 95–102. https://doi.org/10.1016/j.jcis.2013.10.019.

[17] J. Jiang, C. Burger, C. Li, J. Li, M.Y. Lin, R.H. Colby, M.H. Rafailovich, J.C. Sokolov, Shear-induced layered structure of polymeric micelles by SANS, Macromolecules. 40 (2007) 4016–4022. https://doi.org/10.1021/ma062654j.

[18] P. Alexandridis, T. Alan Hatton, Poly(ethylene oxide)poly(propylene oxide)poly(ethylene oxide) block copolymer surfactants in aqueous solutions and at interfaces: thermodynamics, structure, dynamics, and modeling, Colloids and Surfaces A: Physicochemical and Engineering Aspects. 96 (1995) 1–46. https://doi.org/10.1016/0927-7757(94)03028-X.

[19] J. Goodwin, R. Hughes, Rheology for chemists: An Introduction, Royal Society of Chemistry, 2008. https://doi.org/https://doi.org/10.1039/9781847558046.

[20] K. Hyun, J.G. Nam, M. Wilhellm, K.H. Ahn, S.J. Lee, Large amplitude oscillatory shear behavior of PEO-PPO-PEO triblock copolymer solutions, Rheologica Acta. 45 (2006) 239–249. https://doi.org/10.1007/s00397-005-0014-x.

[21] S.C. Millik, A.M. Dostie, D.G. Karis, P.T. Smith, M. McKenna, N. Chan, C.D. Curtis, E. Nance, A.B. Theberge, A. Nelson, 3D printed coaxial nozzles for the extrusion of hydrogel tubes toward modeling vascular endothelium, Biofabrication. 11 (2019). https://doi.org/10.1088/1758-5090/ab2b4d.

[22] W. Zhang, Y. Shi, Y. Chen, J. Ye, X. Sha, X. Fang, Biomaterials Multifunctional Pluronic P123 / F127 mixed polymeric micelles loaded with paclitaxel for the treatment of multidrug resistant tumors, Biomaterials. 32 (2011) 2894–2906. https://doi.org/10.1016/j.biomaterials.2010.12.039.

[23] C. Wu, A.K. Gaharwar, B.K. Chan, G. Schmidt, Mechanically Tough Pluronic F127 / Laponite Nanocomposite Hydrogels from Covalently and Physically Cross-Linked Networks, Macromolecules. 44 (2011) 8215–8224. https://doi.org/10.1021/ma200562k.

[24] S. Bhusari, J. Kim, K. Polizzi, S. Sankaran, A. del Campo, Encapsulation of bacteria in bilayer Pluronic thin film hydrogels: A safe format for engineered living materials, Biomaterials Advances. 145 (2023). https://doi.org/10.1016/j.bioadv.2022.213240.

[25] H. Priks, T. Butelmann, A. Illarionov, T.G. Johnston, C. Fellin, T. Tamm, A. Nelson, R. Kumar, P.J. Lahtvee, Physical Confinement Impacts Cellular Phenotypes within Living Materials, ACS Applied Bio Materials. 3 (2020) 4273–4281. https://doi.org/10.1021/acsabm.0c00335.

[26] M. Lufton, O. Bustan, B. hen Eylon, E. Shtifman-Segal, T. Croitoru-Sadger, A. Shagan, A. Shabtay-Orbach, E. Corem-Salkmon, J. Berman, A. Nyska, B. Mizrahi, Living Bacteria in Thermoresponsive Gel for Treating Fungal Infections, Advanced Functional Materials. 28 (2018) 1801581. https://doi.org/10.1002/adfm.201801581.

[27] P. Bertsch, L. Andrée, N.H. Besheli, S.C.G. Leeuwenburgh, Colloidal hydrogels made of

gelatin nanoparticles exhibit fast stress relaxation at strains relevant for cell activity, Acta Biomaterialia. 138 (2022) 124–132. https://doi.org/10.1016/j.actbio.2021.10.053.

[28] M. Dinkgreve, J. Paredes, M.M. Denn, D. Bonn, On different ways of measuring “the” yield stress, Journal of Non-Newtonian Fluid Mechanics. 238 (2016) 233–241. https://doi.org/10.1016/j.jnnfm.2016.11.001.

[29] S.S. Sagiri, V.K. Singh, S. Kulanthaivel, I. Banerjee, P. Basak, M.K. Battachrya, K. Pal, Stearate organogel-gelatin hydrogel based bigels: Physicochemical, thermal, mechanical characterizations and in vitro drug delivery applications, Journal of the Mechanical Behavior of Biomedical Materials. 43 (2015) 1–17. https://doi.org/10.1016/j.jmbbm.2014.11.026.

[30] T. Iyo, Y. Maki, N. Sasaki, M. Nakata, Anisotropic viscoelastic properties of cortical bone, Journal of Biomechanics. 37 (2004) 1433–1437. https://doi.org/10.1016/j.jbiomech.2003.12.023.

[31] M. Zabet, S. Mishra, S. Kundu, Effect of graphene on the self-assembly and rheological behavior of a triblock copolymer gel, RSC Advances. 5 (2015) 83936–83944. https://doi.org/10.1039/c5ra13672e.

[32] Y. Jia, K. Peng, X.L. Gong, Z. Zhang, Creep and recovery of polypropylene/carbon nanotube composites, International Journal of Plasticity. 27 (2011) 1239–1251. https://doi.org/10.1016/j.ijplas.2011.02.004.

[33] S. Nam, J. Lee, D.G. Brownfield, O. Chaudhuri, Viscoplasticity Enables Mechanical Remodeling of Matrix by Cells, Biophysical Journal. 111 (2016) 2296–2308. https://doi.org/10.1016/j.bpj.2016.10.002.

[34] X. Hong, J.P. Stegemann, C.X. Deng, Microscale characterization of the viscoelastic properties of hydrogel biomaterials using dual-mode ultrasound elastography, Biomaterials. 88 (2016) 12–24. https://doi.org/10.1016/j.biomaterials.2016.02.019.

[35] H.L. Ornaghi, J.H.S. Almeida, F.M. Monticeli, R.M. Neves, Stress relaxation, creep, and recovery of carbon fiber non-crimp fabric composites, Composites Part C: Open Access. 3 (2020) 100051. https://doi.org/10.1016/j.jcomc.2020.100051.

[36] T.H. Qazi, V.G. Muir, J.A. Burdick, Methods to Characterize Granular Hydrogel Rheological Properties, Porosity, and Cell Invasion, ACS Biomaterials Science and Engineering. 8 (2022) 1427–1442. https://doi.org/10.1021/acsbiomaterials.1c01440.

[37] E. Dickinson, Structure and rheology of colloidal particle gels: Insight from computer simulation, Advances in Colloid and Interface Science. 199–200 (2013) 114–127. https://doi.org/10.1016/j.cis.2013.07.002.

[38] G.J. Donley, P.K. Singh, A. Shetty, S.A. Rogers, Elucidating the G'' overshoot in soft materials with a yield transition via a time-resolved experimental strain decomposition, PNAS. 117 (2020) 21945–21952. https://doi.org/10.1073/pnas.2003869117.

[39] M. Malmeten, B. Lindman, Self-Assembly in Aqueous Block Copolymer Solutions, Macromolecules. 25 (1992) 5440–5445.

[40] K.S. Fancey, A mechanical model for creep, recovery and stress relaxation in polymeric materials, Journal of Materials Science. 40 (2005) 4827–4831. https://doi.org/10.1007/s10853-005-2020-x.

[41] H. Tsurusawa, M. Leocmach, J. Russo, H. Tanaka, Direct link between mechanical stability in gels and percolation of isostatic particles, Science Advances. 5 (2019) 1–8. https://doi.org/10.1126/sciadv.aav6090.

[42] L.C. Hsiao, R.S. Newman, S.C. Glotzer, M.J. Solomon, Role of isostaticity and load-bearing microstructure in the elasticity of yielded colloidal gels, Proceedings of the National Academy of Sciences of the United States of America. 109 (2012) 16029–16034. https://doi.org/10.1073/pnas.1206742109.

[43] M.Y. Lin, H.M. Lindsay, D.A. Weitz, R.C. Ball, R. Klein, P. Meakin, Universality in colloid aggregation, Nature. 339 (1989) 360–362. https://doi.org/10.1038/339360a0.

[44] H. Tsurusawa, S. Arai, H. Tanaka, A unique route of colloidal phase separation yields stress-free gels, Science Advances. 6 (2020) 1–11. https://doi.org/10.1126/sciadv.abb8107.

[45] K.A. Whitaker, Z. Varga, L.C. Hsiao, M.J. Solomon, J.W. Swan, E.M. Furst, Colloidal gel elasticity arises from the packing of locally glassy clusters, Nature Communications. 10

(2019). https://doi.org/10.1038/s41467-019-10039-w.

[46] C.R. López-Barrón, N.J. Wagner, L. Porcar, Layering, melting, and recrystallization of a close-packed micellar crystal under steady and large-amplitude oscillatory shear flows, Journal of Rheology. 59 (2015) 793–820. https://doi.org/10.1122/1.4917542.

[47] B. Nyström, H. Walderhaug, F.K. Hansen, Dynamic light scattering and rheological studies of thermoreversible gelation of a poly(ethylene oxide)-poly(propylene oxide)-poly(ethylene oxide) triblock copolymer in aqueous solution, Faraday Discussions. 101 (1995) 335–344. https://doi.org/10.1039/FD9950100335.

[48] L. Mohan, M. Cloitre, R.T. Bonnecaze, Build-up and two-step relaxation of internal stress in jammed suspensions, Journal of Rheology. 59 (2015) 63–84. https://doi.org/10.1122/1.4901750.

[49] T. Murakami, T. Kawamori, J.D. Gopez, A.J. McGrath, D. Klinger, K. Saito, Synthesis of PEO-based physical gels with tunable viscoelastic properties, Journal of Polymer Science, Part A: Polymer Chemistry. 56 (2018) 1033–1038. https://doi.org/10.1002/pola.28992.

[50] C.R. López-Barrón, R. Chen, N.J. Wagner, P.J. Beltramo, Self-Assembly of Pluronic F127 Diacrylate in Ethylammonium Nitrate: Structure, Rheology, and Ionic Conductivity before and after Photo-Cross-Linking, Macromolecules. 49 (2016) 5179–5189. https://doi.org/10.1021/acs.macromol.6b00205.

[51] M. Osawa, H.P. Erickson, Turgor pressure and possible constriction mechanisms in bacterial division, Frontiers in Microbiology. 9 (2018) 1–7. https://doi.org/10.3389/fmicb.2018.00111.

[52] E.K. Chu, O. Kilic, H. Cho, A. Groisman, A. Levchenko, Self-induced mechanical stress can trigger biofilm formation in uropathogenic Escherichia coli, Nature Communications. 9 (2018). https://doi.org/10.1038/s41467-018-06552-z.